

# IDENTIFICATION OF LITHIUM ISOTOPES USING TIME-TAGGED NEUTRON SCATTERING\*

B. R. Grogan, J. T. Mihalcz

Oak Ridge National Laboratory, P.O. Box 2008, MS-6010, Oak Ridge, TN 37831-6010, USA

E-Mail Addresses: [groganbr@ornl.gov](mailto:groganbr@ornl.gov), [mihalczajt@ornl.gov](mailto:mihalczajt@ornl.gov)

## ABSTRACT

Lithium deuteride and hydride salts enriched in the  ${}^6\text{Li}$  isotopes are integral components of thermonuclear weapons. Since 1963, the United States has not had an operational facility for enriching lithium. It is therefore important to ensure that existing stocks of this material are properly identified and stored for future contingencies. This work shows that time-tagged neutron scattering can be used to measure the hydrogen isotope and the lithium enrichment of the materials in storage containers nonintrusively. Performing verification measurements in this manner is likely to be cheaper and less hazardous than opening the containers for a destructive assay. Using a deuterium-tritium (D-T) generator to produce time-tagged and electronically collimated 14 MeV neutrons, the time of flight to travel to an object and then scatter into a detector is a particularly useful signature for determining the light isotope composition in an object. Another useful signature produced by time-tagged neutron scattering is the characteristic gamma rays produced by inelastic scattering reactions. Using Monte Carlo simulations, this conceptual study will show that the time of flight is an excellent method for measuring both the hydrogen isotopic abundances, and that both signatures can be used to measure the lithium enrichment.

## INTRODUCTION

Lithium enriched in the isotope  ${}^6\text{Li}$  can be used for tritium production, and as a component in nuclear weapons [1]. In the latter role, the lithium is typically found in the form of the salts lithium hydride (LiH) or lithium deuteride (LiD) [2]. Natural lithium contains only 7.5%  ${}^6\text{Li}$ , while the remaining 92.5% is  ${}^7\text{Li}$ , by isotopic abundance. Lithium enrichment operations in the United States were conducted primarily at the Y-12 Colex (column exchange) facility between 1955 and 1963 [3]. Since the shutdown of that facility in 1963, there has been no operational lithium enrichment in the United States. It is therefore essential that enriched lithium salts on hand be properly identified and safeguarded so that they will be available for any future contingencies.

Determination of the lithium enrichment and the hydrogen isotopic form (hydride or deuteride) of lithium salts on hand could be verified using traditional destructive analysis techniques; however, this procedure requires opening the storage container and direct contact with the material. Because lithium salts are highly reactive, special precautions would have to be taken, which could make the cost of such an operation significant. Performing this procedure on a large number of containers would likely be cost prohibitive and manpower intensive. Time-tagged neutron scattering offers a method that can be used to verify these materials without the need to open the containers or come into direct contact with the lithium salts.

---

\* This manuscript has been authored by UT-Battelle, LLC, under contract DE-AC05-00OR22725 with the U.S. Department of Energy. The United States Government retains and the publisher, by accepting the article for publication, acknowledges that the United States Government retains a non-exclusive, paid-up, irrevocable, worldwide license to publish or reproduce the published form of this manuscript, or allow others to do so, for United States Government purposes.

## THEORY

Time-tagging refers to the technique of recording the time at which each neutron of interest is produced (the start time). By time-tagging the neutrons in this manner, the time a neutron arrives in a distant detector (the stop time) can be used to measure its time of flight. One common method of time-tagging neutrons is to detect one of the other products from the reaction that produced the neutron. A deuterium-tritium (D-T) neutron generator produces neutrons via the  ${}^3\text{H}({}^2\text{H},\text{n}){}^4\text{He}$  reaction. The neutrons are produced isotropically with a kinetic energy of 14.1 MeV. The alpha particle ( ${}^4\text{He}$  nucleus) produced in this reaction is a heavy charged particle that easily interacts with a thin detector. In contrast, the detector is almost completely transparent to the neutrons, making the number of “false alpha” detections low. Because the neutron and alpha particle are produced essentially back-to-back, the geometry of the alpha detector and the target spot where the D-T reaction occurs also electronically collimates the neutrons. This electronic collimation eliminates a large portion of the active background that would normally be produced by out-of-cone neutrons scattering or inducing secondary radiation that returns to the detector some time later. Because these neutrons are not correlated with an in-cone alpha particle, they appear as a uniform background signal that can be subtracted from the measured time-of-flight curves.

One of the most common measurements performed with time-tagged neutrons is neutron radiography. Two measurements make use of the neutrons that travel through the object without interacting. Two measurements are made—one with the object of interest between the neutron source and a position-sensitive detector and another without the object. The attenuation of neutrons through the object is calculated as a function of detector position, and using the source-object-detector geometry, a three-dimensional tomograph of the object can be reconstructed. This tomograph shows the attenuation coefficient for each voxel inside of the object for the incident neutron energy. While this information is extremely useful for distinguishing certain classes of materials (e. g., steel from polyethylene), the attenuation coefficients are not unique to a particular material. Thus, additional information is required to make a positive identification of the materials inside the object. Neutron radiography has been presented in several previous papers [4–7], and it will not be discussed further in this work.

For fast ( $>1$  MeV) neutrons that are not transmitted through the object, the primary interactions with light nuclei are elastic and inelastic scattering. Elastic scattering is a billiard-ball-like collision in which kinetic energy is conserved. In contrast, an inelastic collision is one in which some of the neutron’s kinetic energy is converted to raise the target nucleus to an excited energy level. This excitation energy is referred to as the Q-value of the reaction, which is a negative value because the reaction is endothermic. The Q-values of each nuclide are unique. For some of the very lightest isotopes ( ${}^1\text{H}$  and  ${}^4\text{He}$ ), no excited states exist, and so only elastic scattering is possible. For other light isotopes, the energy levels tend to be widely spaced and easily distinguishable. For a given incident neutron energy ( $E_i$ ), scattering isotope atomic mass ( $A$ ), scattering angle ( $\theta_L$ ), and Q-value ( $Q$ ), the final neutron energy ( $E_f$ ) is uniquely determined via the equation

$$E_f = \frac{1}{(A+1)^2} \left[ \cos(\theta_L) \sqrt{E_i} + \sqrt{E_i(\cos^2(\theta_L) + A^2 - 1) + A(A-1)Q} \right]^2. \quad (1)$$

For the case of elastic scattering,  $Q = 0$ .

Because D-T neutrons are monoenergetic, the time required for them to travel a given distance to the target, scatter, and travel another distance to a detector at a given angle can be exactly determined using Equation 1. For example, a 14.1 MeV neutron travelling at 5.14 cm/ns scattering from a  ${}^6\text{Li}$  nucleus at an

angle of  $135^\circ$  will have a final kinetic energy of 7.93 MeV and a speed of 3.87 cm/ns. Table 1 shows the time of flight for a 14.1 MeV neutron to travel 50 cm from its source location (approximately 10 ns), scatter through a given angle, and then travel 300 cm to a detector. The times of flight for elastic scattering and inelastic scattering to prominent energy levels are shown for the naturally occurring hydrogen and lithium nuclei. Elastic scattering values are also given for several heavier isotopes for reference. Note that for elastic scattering, the best resolution between different masses is obtained at the greatest scattering angles because the neutron energy loss is greatest.

Table 1. Time of flight for a 14.1 MeV neutron to travel 50 cm, scatter from a nucleus at the indicated angle, and travel to a detector 300 cm away. The inelastic Q-values used are the energy levels of the  ${}^6\text{Li}$  and  ${}^7\text{Li}$  isotopes. Mass numbers with no Q-value represent elastic scattering.

Mass Number (Q-Value)	t @ $45^\circ$ (ns)	t @ $90^\circ$ (ns)	t @ $135^\circ$ (ns)	t @ $180^\circ$ (ns)
1	91.9	--	--	--
2	77.5	110.2	158.9	183.2
7 (-4630 keV)	84.8	95.1	106.8	112.0
6 (-3562 keV)	81.2	92.1	104.6	110.2
6 (-2186 keV)	76.7	86.0	96.6	101.4
6	71.0	78.6	87.2	91.1
7 (-478 keV)	71.7	78.3	85.7	89.0
7	70.6	77.0	84.1	87.2
16	69.2	71.8	74.6	75.8
40	68.6	69.6	70.6	71.1
100	68.3	68.7	69.1	69.3
208	68.2	68.4	68.6	68.7

In addition to the neutron time of flight, another useful measurement with time-tagged neutron scattering is gamma spectroscopy. After an inelastic scatter leaves the nucleus in an excited state, it decays to the ground state in a time on the order of picoseconds or less. This time is much shorter than the time resolution of the scintillators modeled in this work, so it is essentially instantaneous. The decay produces gamma rays with energies that are characteristic of the decaying nuclide. The presence and relative intensity of these characteristic gamma rays can be used to confirm the presence of those nuclides and measure their relative isotopic abundance.

## SIMULATION PROCEDURE

For this study, time-tagged neutron scattering measurements were simulated using Monte Carlo N-Particle (MCNP) software. For the neutron time-of-flight simulations, a beta version of MCNPX-PoliMi [8], version 1.4.3, was used. For the gamma spectroscopy simulations, MCNPX version 2.6.0 [9] was used. The lithium salts were assumed to be in a small sphere with a radius of 5 cm. For LiH, the density was assumed to be  $0.82 \text{ g/cm}^3$ , and for LiD, the density was assumed to be  $0.92 \text{ g/cm}^3$ . A LiH/LiD sphere of this size and density would weigh between 400 and 500 g. The LiD was modeled with  ${}^6\text{Li}$  enrichments of 0, 7.5 (natural), 20, 40, 60, 80, and 100 percent; LiH with a natural  ${}^6\text{Li}$  enrichment was also modeled.

The D-T source was modeled as a  $5.7^\circ$  wide cone of 14.1 MeV neutrons located 50 cm from the lithium target. This cone subtends 0.25% of the total spherical solid angle, and it is completely subtended by the target. In practical applications for larger targets, several pixels of this size could be used to define neutrons on the target and reduce measurement time. A plastic scintillator with an active volume of  $25 \times 25 \times 8 \text{ cm}$  was located 300 cm from the center of the target at an angle of  $135^\circ$  relative to the centerline of the neutron cone. The scintillating material was enclosed in a 1 cm thick aluminum case. An 8.31 cm long

× 7.73 cm diameter high-purity germanium (HPGe) detector was located 50 cm from the lithium target at an angle of  $90^\circ$  relative to the neutron cone. The geometry of the neutron cone, LiH/LiD target, and detectors is shown in Figure 1.

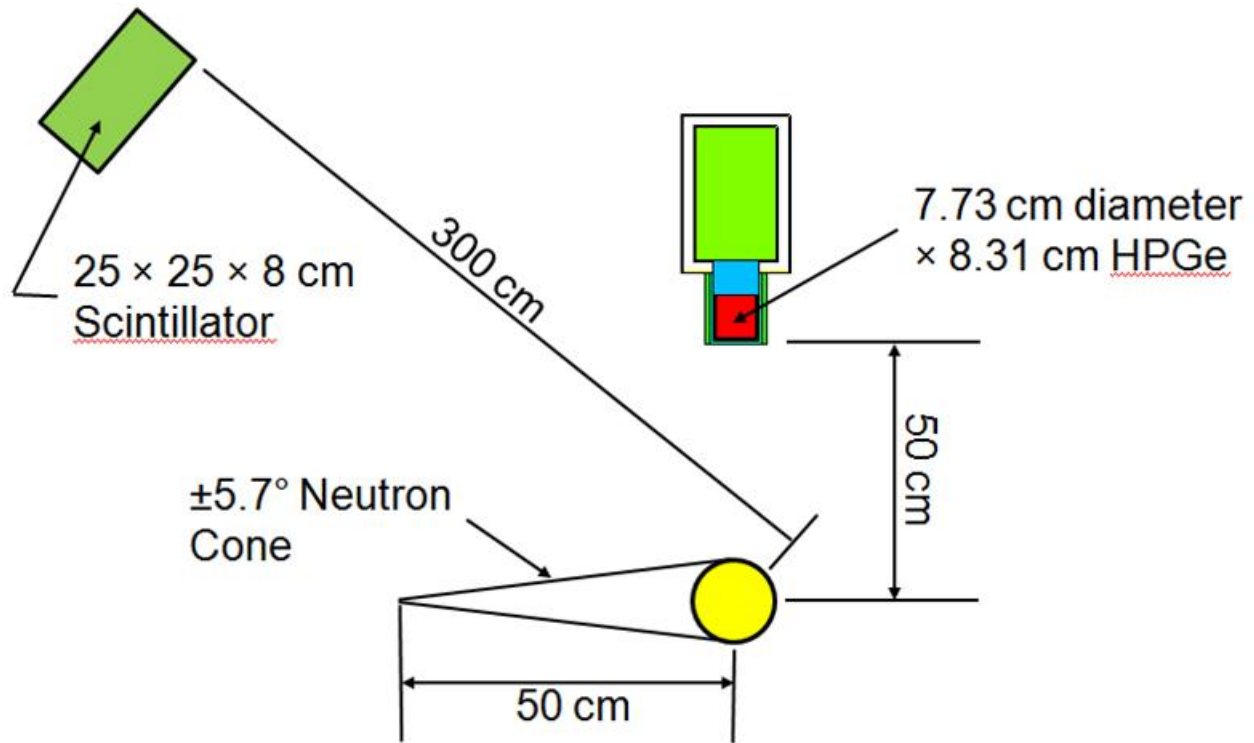


Figure 1. The source, LiD/LiH target, and detector geometry used for simulations.

For the time-of-flight simulations,  $2 \times 10^9$  source histories were simulated for each scenario. This is equivalent to 2.2 hours of measurement time using one pixel of an alpha detector for a neutron generator with a source strength of  $10^8$  neutrons per second. The MCNPX-PoliMi simulations generated list mode files with the time, interaction type, and energy deposited by each collision in the simulated scintillator crystal. This file was post-processed with software written by one of the authors [BRG] to calculate the light output produced by each interaction in order to generate detector pulses. The energy deposition to light conversion values were taken from Ref. 10. A threshold equivalent to the maximum light output of a 1 MeV neutron was applied to all calculated pulses. In addition, a Normally distributed timing uncertainty of  $\pm 1$  ns was applied to both the source time (simulating uncertainty in the alpha detector) and the plastic scintillator. The resulting pulses were binned into 1 ns intervals to produce the final neutron time-of-flight data.

For the gamma spectroscopy simulations, each scenario consisted of  $1 \times 10^9$  source histories, equivalent to 1.1 hours of measurement time with a  $10^8$  neutron per second generator. An F8 (pulse height) tally was used to generate the light output in the HPGe crystal. The tally binned the pulse height into 8192 equally spaced bins between 0 and 6 MeV. A Gaussian energy broadening (GEB) card was used to give the tally the desired energy resolution using the formula

$$FWHM = a + \sqrt{b + cE^2}, \quad (2)$$

where E is the gamma energy, and FWHM is the full width at half maximum of resulting peak, both in units of MeV. The three coefficients used in Equation 2 were  $a = 0.00372$ ,  $b = 5.0964 \times 10^{-5}$ , and  $c = 0$ . These values simulate an energy resolution (FWHM / E) of 0.75% at 661 keV. The resulting spectra were analyzed using the PeakEasy 3.85 software [11] to determine the net counts under each peak.

## RESULTS

### Neutron Time-of-Flight

Figure 2 shows the time-of-flight curves for three enrichments of LiD and natural LiH over a time lag range of 70–175 ns after neutron production. The major peaks in each of the curves are labeled, along with the expected time of flight (using Equation 1) and the reaction(s) responsible for the peak. The lack of the large elastic scattering peak at 159 ns clearly differentiates the LiH sample from the LiD. Because of the ease with which the two hydrogen isotopes can be identified, the majority of this work focuses on determining the lithium enrichment in LiD. Although the peak at 85 ns clearly shifts to a longer lag time between the 0% and 100%  $^6\text{Li}$  enrichment scenarios, the time resolution simulated in the measurement is not sufficient to resolve the two elastic scattering peaks and the 478 keV  $^7\text{Li}$  inelastic scattering peak when both isotopes are present (note the 40%LiD curve). Because of this, the ratios of the two elastic scattering peaks alone cannot be used to calculate the isotopic abundance of  $^6\text{Li}$  in the sample.

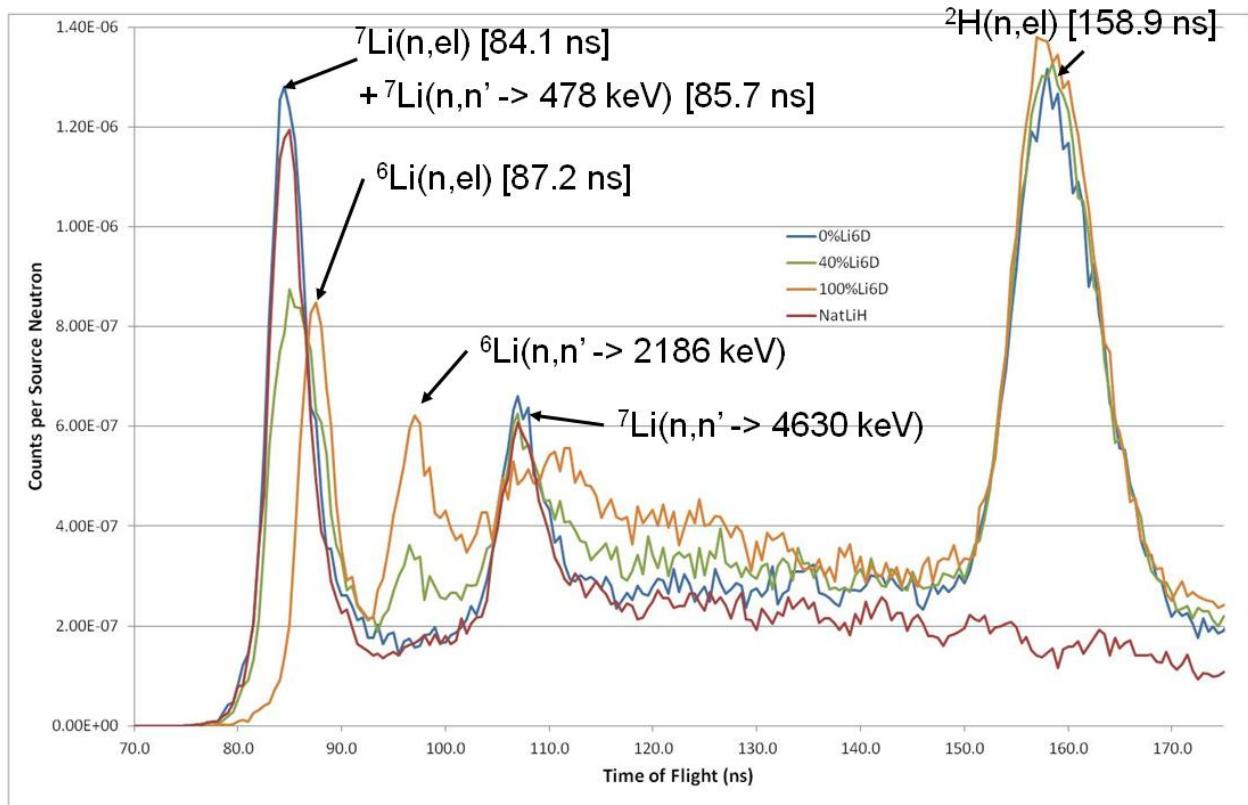


Figure 2. Time-of-flight curves produced by neutrons scattering from natural LiH and three different enrichments of LiD.

The time-of-flight plot was subsequently divided into six regions, as shown in Figure 3. The six regions were chosen manually in order to maximize the contrast due to the respective peaks. All possible ratios of counts between each of the regions were computed to determine which were sensitive to the  ${}^6\text{Li}$  enrichment or the hydrogen isotope. The ratios of R3/R6 and R5/R6 were found to be particularly insensitive to the enrichment, but very sensitive to the presence of the hydride or deuteride forms. Thus, these ratios could be used to determine if some or all of the lithium salt in the sample consists of LiH rather than LiD. Conversely, the ratio of R1/R2 is a good indicator of the lithium enrichment for LiD. The three ratios are shown in Figure 4. The relationship between the R1/R2 ratio and the  ${}^6\text{Li}$  enrichment was fitted with an exponential of the form  $\%{}^6\text{Li} = -17.37 + 204.5e^{-0.5291R1/R2}$ . This fit produces an accurate estimate of the enrichment over the entire range from 0–100%  ${}^6\text{Li}$ . Using these three ratios, the lithium salts can first be checked to determine if they consist of LiH or LiD, and if they are LiD, an estimate of the enrichment can be made. Estimates of the lithium enrichment in LiH were not tested in this work, but they would be expected to follow a similar trend.

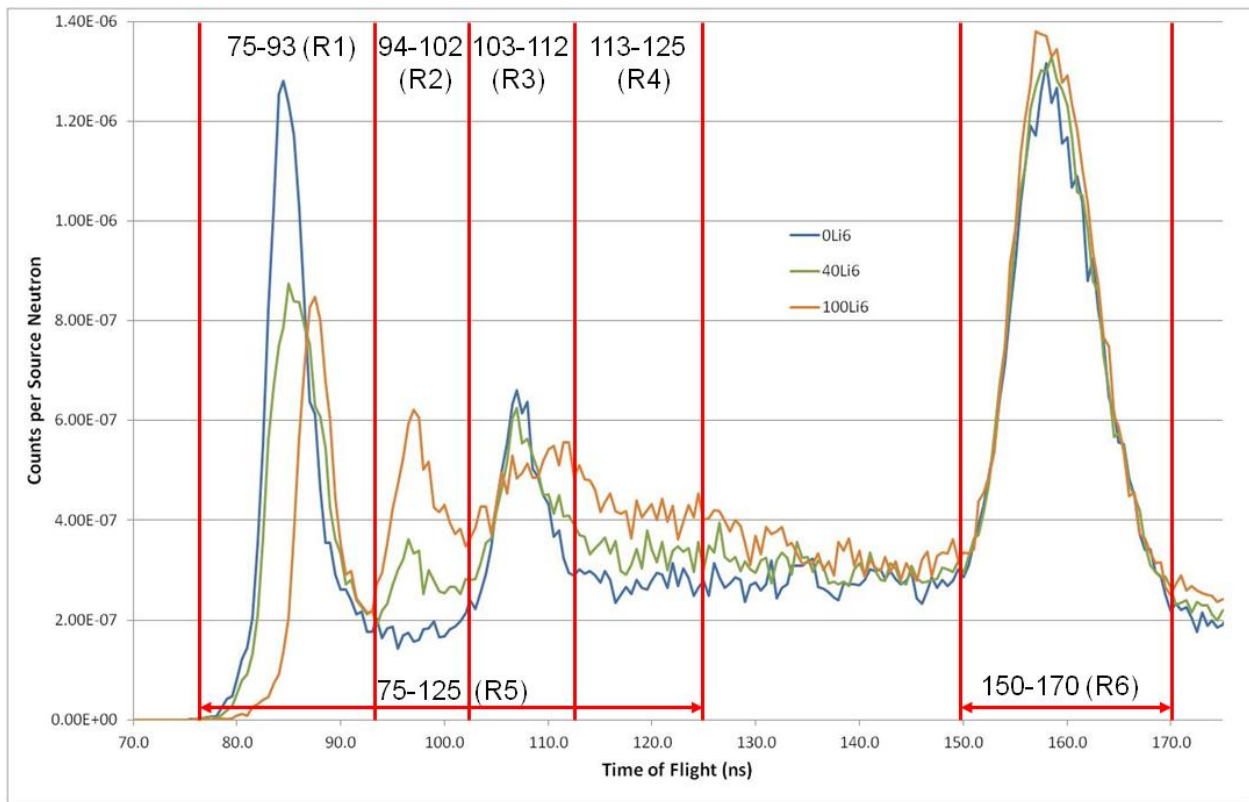


Figure 3. Time-of-flight curves for LiH and LiD with the six defined regions overlaid. The label for each region includes the time lag boundaries in ns.

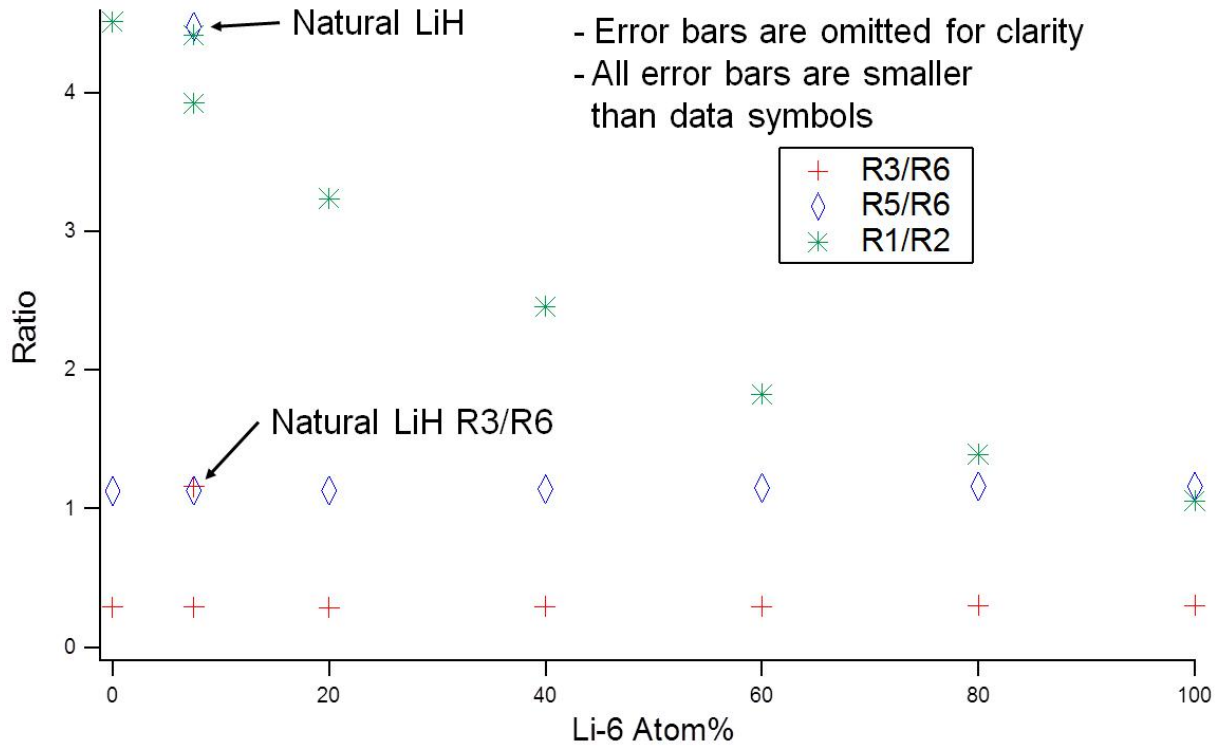


Figure 4. Plot of the three time-of-flight region ratios of interest. All data shown are for LiD except for the indicated natural (7.5%  $^6\text{Li}$ ) LiH point. Ratios R3/R6 and R5/R6 are very sensitive to the form of the hydrogen isotope (light hydrogen or deuterium), while R1/R2 is primarily sensitive to the  $^6\text{Li}$  enrichment.

### GAMMA SPECTROSCOPY

Figure 5 shows the gamma spectra produced by the active interrogation of LiD enriched at 0% and 100%  $^6\text{Li}$  with D-T neutrons. The  $^6\text{Li}$ D spectrum is offset from the x-axis for clarity. Of the peaks in these spectra, only two are produced by lithium nuclei: the 478 keV  $^7\text{Li}$  peak and the 3562 keV  $^6\text{Li}$  peak. The other peaks are produced by materials such as the aluminum detector housing or the photomultiplier tube.

Figure 6 shows a plot of the ratio of net counts under the 478 keV peak and 3562 keV peak versus the  $^6\text{Li}$  enrichment. An exponential fit of the data points is also shown. That fit takes the form

$$\text{Li - 6 Enrichment} = 102.8e^{-0.007284 \times \text{Ratio}(478/3562)} \quad (3)$$

where  $\text{Ratio}(478/3562)$  is the ratio of the net counts under the 478 keV and 3562 keV peaks. Note that this fit does an excellent job predicting the enrichment at values above 20%, but below that value, the scarcity of 3562 keV counts makes the fit unreliable. Therefore, any predicted enrichment below 20% should be considered statistically indistinguishable from natural LiD using this method alone.

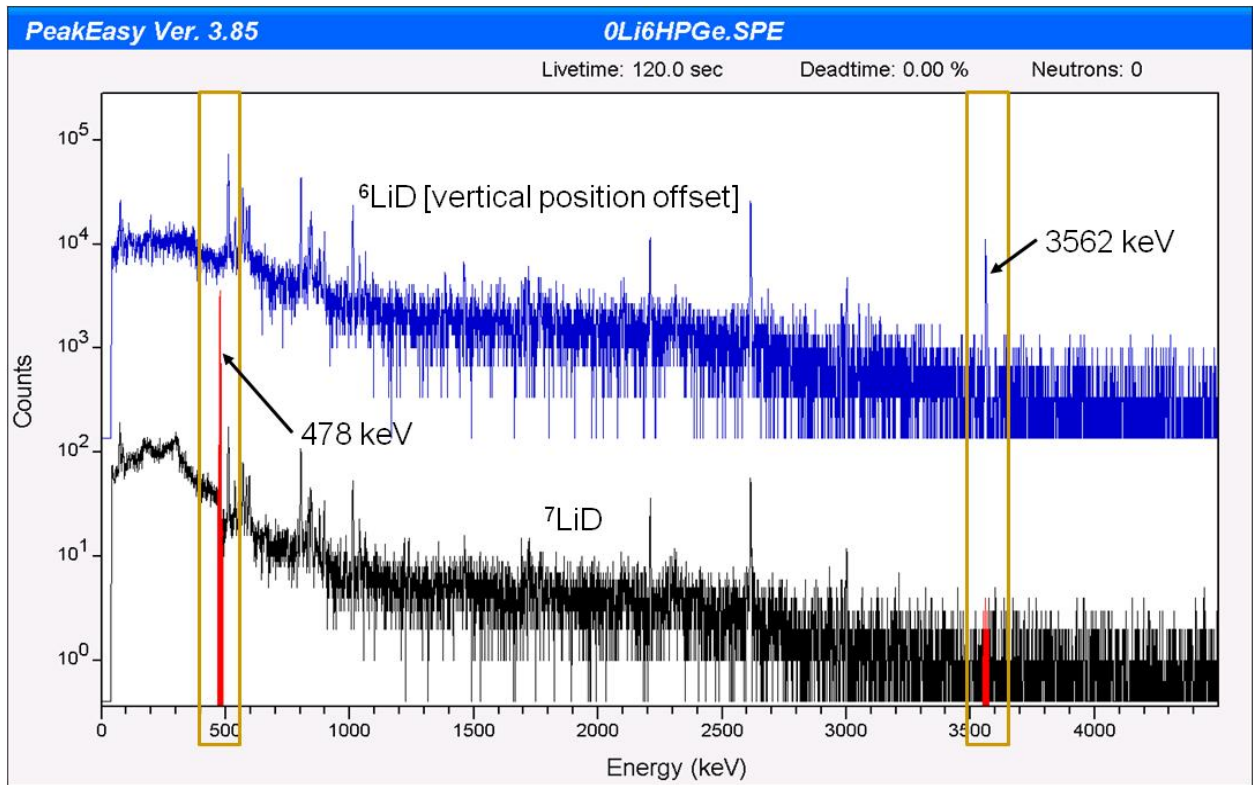


Figure 5. Gamma spectra for  ${}^6\text{LiD}$  and  ${}^7\text{LiD}$ . The  ${}^6\text{LiD}$  spectrum is offset from the x-axis for clarity. Only two peaks at 478 and 3562 keV distinguish the two spectra.

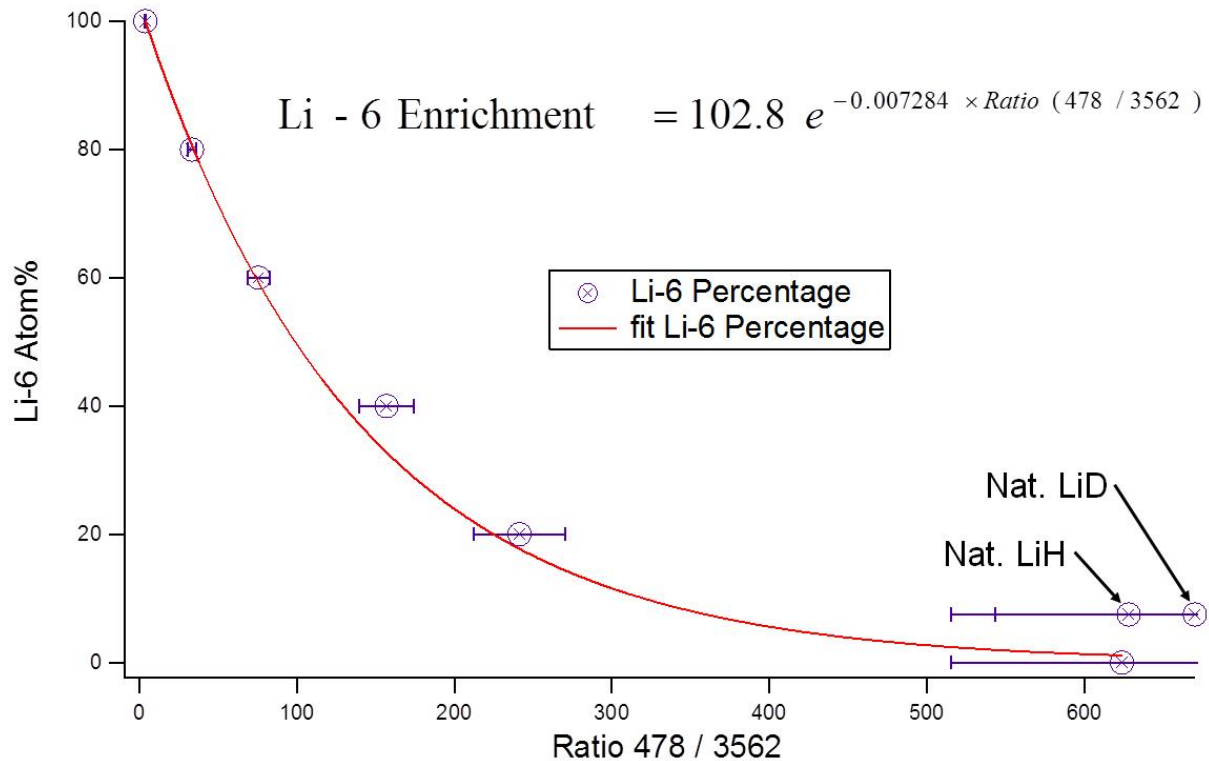


Figure 6. Plot of the  ${}^6\text{Li}$  enrichment in LiD vs. the ratio of net counts in the 478 keV and 3562 keV peaks. Natural LiH and LiD were not used to generate the fit, but are shown for reference.

## CONCLUSIONS AND RECOMMENDATIONS FOR FUTURE WORK

This study has presented a proof-of-concept showing that time-tagged neutron scattering can be used to determine the chemical form and enrichment of LiH and LiD. The presence or absence of the deuterium elastic scattering peak (quantified by the ratios of counts in regions R3/R6 or R5/R6) can be used to determine if the lithium salt is in a hydride or deuteride form. If the material is shown to be in a deuteride form, the ratio of counts in regions R1/R2 is an excellent predictor of enrichment. Simultaneous measurements of the active gamma spectra can also be used to estimate the  ${}^6\text{Li}$  enrichment using the ratio of the 478 and 3562 keV peaks at enrichments above about 20%. Although not specifically tested in this work, the lithium enrichment in LiH would be expected to produce the same trends in the time-of-flight and gamma spectroscopy ratios as the LiD scenarios, albeit with different fit coefficients. These techniques offer a method for accurately characterizing these materials at a lower cost and with less risk than opening the containers for a destructive assay.

This conceptual study used an ideal measurements system with no concern about measurement time. For practical implementation, use of additional pixels of the alpha detector, closer spacing of the generator and the target, slightly shorter flight path to the neutron detector, use of additional detectors at different angles, and use of DT generator with increased output will have to be investigated. These improvements could lead to measurement times of 10 minutes or less. While this work has shown that the methods simulated can accurately characterize lithium salts, the actual measured values will depend on a great number of variables, such as the source and detector geometry, detector types and gain settings, container composition, etc. Therefore, experimental measurements will be necessary to validate these measurement techniques, and to establish empirical values for fit coefficients. These measurements would also serve to optimize the geometry, detector settings, and time lag boundaries of the regions used in constructing the ratios in order to maximize the accuracy and sensitivity of the methods developed here.

## REFERENCES

1. U.S. Department of Energy, Office of the Press Secretary, *Declassification of the Quantity of Enriched Lithium Produced at the Y-12 Plant in Oak Ridge, Tennessee*, <https://www.osti.gov/opennet/forms.jsp?formurl=document/press/pc23.html> (accessed April 2012).
2. S. O. Cox, *Criteria for the Safe Storage of Lithium Metal and Lithium Compounds at the Y-12 Plant*, Y/ES-013, Oak Ridge Y-12 Plant, Oak Ridge, TN, 1995.
3. U.S. Department of Energy, Office of Environmental Management, *Linking Legacies: Connecting the Cold War Nuclear Weapons Production Processes to Their Environmental Consequences*, DOE/EM-0319, Washington, D.C., 1997.
4. J. A. Mullens, *Addition of Tomographic Capabilities to NMIS*, Y/LB-16,160, Y-12 National Security Complex, Oak Ridge, TN, 2003.
5. P. A. Hausladen et al., "Portable fast neutron radiography with the nuclear materials identification system for fissile material transfers," *Nuclear Instruments and Methods in Physics Research B* **261**, 387–390 (2007).
6. B. R. Grogan et al., "Identification of Shielding Material Configurations Using NMIS Imaging," Proceedings of the 52<sup>nd</sup> Annual Meeting of the International Nuclear Materials Management, Palm Desert, CA, July 2011.
7. B. R. Grogan, *The Development of a Parameterized Scatter Removal Algorithm for Nuclear Materials Identification System Imaging*, ORNL/TM-2010/65, Oak Ridge National Laboratory, 2010.
8. E. Padovani et al., MCNPX-PoliMi Users Manual, Release 2.0.0 is available through the Radiation Safety Information Computational Center, <http://rsicc.ornl.gov>.
9. D. B. Pelowitz ed., *MCNPX User's Manual, Version 2.6.0*, LA-CP-07-1473, Los Alamos National Laboratory, Los Alamos, NM, 2008.
10. S. A. Pozzi et al., "Analysis of neutron and photon detection position for the calibration of plastic (BC-420) and liquid (BC-501) scintillators," *Nuclear Instruments and Methods in Physics Research A* **524**, 92–101 (2004).
11. *N-2/N-2 PeakEasy Home Web Page*, <http://peakeasy.lanl.gov> (accessed April 2012) [Limited to U.S. Government affiliates].